Journal of Alloys and Compounds 504S (2010) S472–S475

Contents lists available at ScienceDirect

Journal of Alloys and Compounds

journal homepage: www.elsevier.com/locate/jallcom

Mechanical properties of rapidly solidified Fe–Al–B ternary alloys

Ran Li[a,b,*], Shujie Pang[b], Mihai Stoica[a], Jin Man Park[a], Uta Kühn[a], Tao Zhang[b], Jürgen Eckert[a,c]

[a] Institute for Complex Materials, IFW Dresden, P.O. Box 27 01 16, D-01171 Dresden, Germany
[b] Department of Materials Science and Engineering, Beijing University of Aeronautics and Astronautics, Beijing 100083, China
[c] Institute of Materials Science, TU Dresden, D-01062 Dresden, Germany

ARTICLE INFO

Article history:
Received 21 August 2009
Received in revised form 18 January 2010
Accepted 10 February 2010
Available online 18 February 2010

Keywords:
Transition metal alloys and compounds
Rapid solidification
Mechanical properties
X-ray diffraction

ABSTRACT

In this work, the influence of Al and B concentration on the constituent phases and the mechanical properties of $Fe_{100-x-y}Al_xB_y$ ($0 < x \leq 35$, $0 < y \leq 25$, and $x + y \leq 50$) ternary alloys produced by copper mould casting was investigated. In this composition range, the rapidly solidified alloys contain two crystalline phases: α-Fe(Al) solid solution and Fe_2B compound. Contour maps of compressive strength (σ_c) and fracture strain (ε_f) are plotted according to the quasi-static compression test results of the as-cast Fe–Al–B rods. These rapidly solidified Fe–Al–B crystalline alloys, such as $Fe_{55}Al_{30}B_{15}$ as a typical sample, can show an ultra-high σ_c up to ~3 GPa and a certain plasticity (~5%). The formation of ultrafine eutectics and solid-solution strengthening of Al substitutional solution in α-Fe are considered to be responsible for the considerable improvement of strength.

1. Introduction

Recently, much attention has been directed to rapidly solidified multiphase composite alloys, especially Fe-, Al-, and Ti-based alloys with wide potential applications [1–11]. These composites consist of hard and soft phases with an ultrafine microstructure formed during the rapid solidification process, which can result in high strength and controllable deformation behavior. For example, Ti-based multiphase composite alloys consisting of β-Ti solid solution and nano-eutectic matrix produced by copper mold casting show a high strength of ~2 GPa and a large plasticity up to 10% under compressive conditions. Such strength values are comparable to those of Ti-based bulk metallic glasses with similar compositions [1,2]. In addition, high-strength bulk Al-based alloys consisting of deformable Al and hard intermetallic phases, which show largely improved mechanical properties (above 1 GPa strength and up to 150% plasticity) compared to traditional Al-based alloys, were developed using carbon/copper mold casting [3,4]. Fe-based rapidly solidified bulk alloys in the Fe–Cr–Mo–(V,Ga)–C, Fe–Nb–Al, Fe–Zr–(B,Ti) and (Fe–Co)–Mo–C–Si–B systems with a similar soft-hard phase composite structure also exhibit remarkable mechanical properties of ~3 GPa compressive strength and considerable plasticity [5–11]. Therefore, this kind of composite alloys are promising candidates as advanced engineering materials due to the positive combination of the high-strength typical of bulk metallic glasses with the plastic deformation of conventional crystalline materials. The deformation mechanism of this type of soft-hard phase composite alloys has been discussed in many reports [1,2,7,9]. Recently, we provided a fracture model based on the sliding mode of cracks to obtain a quantitative relationship between the mechanical properties and the characteristic microstructure, which can be helpful to design and analyze the fracture behavior of this kind of composites [11].

In the present study, we further extend the studies on the development of rapidly solidified Fe-based composite alloys with novel mechanical properties to the ternary Fe–Al–B system because Fe–Al-based alloys show the great advantage of relatively low density and cheap resources [12–14]. The addition of B in Fe–Al alloys could be beneficial for the formation of ultrafine eutectic phases so as to promote the microstructural characteristics of a soft-hard phase composite. The constituent phases and the compressive mechanical properties of the as-cast rods produced by copper mold casting are evaluated in detail. The strengthening mechanism occurring in the Fe–Al–B samples is described through establishing a relationship between phase composition, microstructure and mechanical properties.

2. Experimental procedure

Pure iron (99.5% purity), electrolytic aluminum (99.999% purity), and crystalline boron (99.8% purity) were used as starting materials. The $Fe_{100-x-y}Al_xB_y$ ($0 < x \leq 35$, $0 < y \leq 25$, and $x + y \leq 50$) ternary alloys were melted using a high-frequency induction furnace in high-purity argon atmosphere. Subsequently, the ingots were cracked into pieces. A lump of these alloys of about 5 g was remelted in a quartz tube using a high-frequency induction device in argon atmosphere, and the molten

* Corresponding author at: Leibniz Institute for Solid State and Materials Research (IFW) Dresden, Helmholtzstraße 20, 01069 Dresden, Germany.
Tel.: +49 351 4659 645.
E-mail address: r.li@ifw-dresden.de (R. Li).

0925-8388/$ – see front matter © 2010 Elsevier B.V. All rights reserved.
doi:10.1016/j.jallcom.2010.02.082

alloys were injected into a copper mould in order to obtain rapidly solidified rod-shape samples with 5 mm diameter and a length of 50 mm. The phases were checked using a RIGAKU RINT-2000 X-ray diffractometer (XRD) with Cu Kα radiation. The thermal properties associated with melting of the samples were measured by high-temperature differential scanning calorimetry (DSC) at a heating rate of 0.33 K/s. The microstructure of the specimens was examined by scanning electron microscopy (SEM). Cylindrical samples with 5 mm diameter and 10 mm length were tested at room temperature at a constant strain rate (1×10^{-4} s^{-1}) under compression using a SANS CMT5504 testing facility.

3. Results and discussion

In the whole tested composition region, only two crystalline phases can be identified for the rapidly solidified Fe–Al–B alloys at the sensitivity of X-ray diffraction. One is a disordered α-Fe(Al) solid solution; the other is the Fe_2B compound. The non-equilibrium fabrication process restricts the formation of the $D0_3$-ordered Fe_3Al intermetallic phase, which normally exists in Fe–Al-based alloys produced under equilibrium conditions [12–14]. In order to elucidate the possible influence of the Al or B concentration on the phase composition, a series of XRD patterns of $Fe_{85-x}Al_xB_{15}$ and $Fe_{80-y}Al_{20}B_y$ alloys is shown in Fig. 1(a) and (b). With the increasing Al content (x) in $Fe_{85-x}Al_xB_{15}$ alloys with a fixed B content, the Bragg peaks of α-Fe(Al) shift towards lower diffraction angles, as shown in Fig. 1(a), which indicates an increase of the lattice parameter of this phase. More Al solute in the α-Fe(Al) solid solution can be responsible for the distortion of the crystal lattice [15]. The effect of the increase in the Al content on the peak shift of Fe_2B is indistinctive. This indicates that the change of Al concentration will not influence the phase composition of Fe_2B. For the $Fe_{80-y}Al_{20}B_y$ alloys with a fixed Al concentration, the increase in B content decreases the intensity of α-Fe(Al), while enhancing the intensity of Fe_2B [Fig. 1(b)], which suggests a lower (higher) volume fraction of α-Fe(Al) and (Fe_2B), respectively, in the corresponding alloys.

The melting behavior of these alloys was evaluated by DSC. The liquidus surface in the Fe–Al–B ternary system shows a "temperature valley". The eutectic point of the Fe–B binary system projects into the Fe–Al–B ternary system as a boundary curve along the contour lines of about 15 at.% B to form this valley. Actually, so far little information on the constituent phase(s) or thermodynamic data (especially at high temperature) are available for the Fe–Al–B system [16]. Combining the information from the Fe–Al and Fe–B binary phase diagrams, the Fe–Al–B ternary system can be simplified as a pseudo-binary eutectic system with two terminals: Fe(Al) solid solution and the Fe_2B compound, because only these two phases can be found in the whole composition region [17]. This assumption was used for the following analysis of the microstructure and the mechanical properties of our samples.

Fig. 2(a) shows some typical compressive strain–stress curves of the as-cast Fe–Al–B alloys. Considering the B content in the samples, the alloys can be divided into three types: hypo-eutectic (B content < 15 at.%), near-eutectic (B content ≈ 15 at.%) and hyper-eutectic (B content > 15%) alloys. The hypo-eutectic alloy, i.e. $Fe_{75}Al_{20}B_5$, exhibits large plastic deformation (ε_p) up to 14%. The yield strength (σ_y) and compressive strength (σ_c) of this alloy are 640 and 1350 MPa, respectively. The as-cast alloys with a composition near to the eutectic point, i.e. $Fe_{85-x}Al_xB_{15}$ (x = 10, 20, 30), show much higher σ_y and σ_c (1.3–1.7 and 1.7–3.0 GPa) but lower plasticity (ε_p of 1.6–5.0%) compared to the hypo-eutectic alloy. When the B content is further increased up to 25 at.% to form the hyper-eutectic alloy, i.e. $Fe_{55}Al_{20}B_{25}$, this alloy shows brittle fracture with σ_c of 2.3 GPa without plastic deformation. The deformation mechanism of hypo-eutectic, near-eutectic and hyper-eutectic alloys has been elaborated in many papers [1,2,7,9,11]. Normally, the high strength is attributed to the supporting framework of a hard network-like

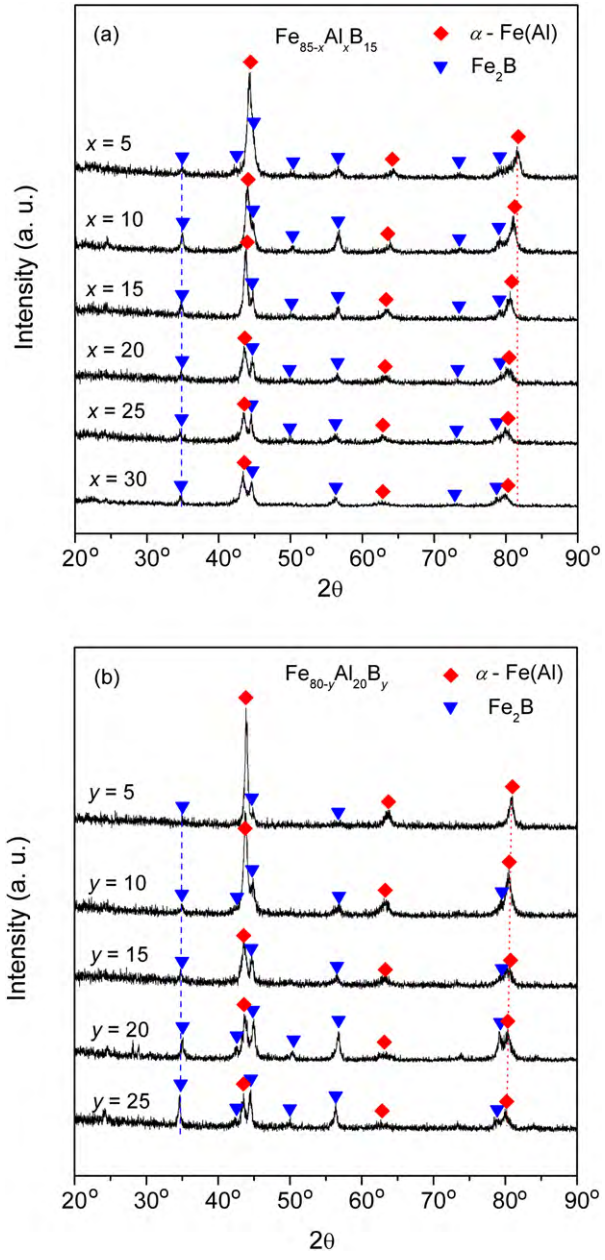

Fig. 1. XRD patterns of rapidly solidified (a) $Fe_{85-x}Al_xB_{15}$ (x = 5, 10, 15, 20, 25 and 30) and (b) $Fe_{80-y}Al_{20}B_y$ (y = 5, 10, 15, 20 and 25) alloys. The red dotted lines and the blue dashed lines are guidelines for the eye to identify a possible peak shift. (For interpretation of the references to color in this figure legend, the reader is referred to the web version of the article.)

ultrafine eutectic, whereas the plasticity is believed to mainly stem from plastically deformable primary dendrites. Because the primary phase in the hyper-eutectic alloy is a brittle intermetallic phase, the catastrophic fracture of this kind of alloys without any plasticity can be easily understood. These results indicate that the mechanical properties, such as strength and plasticity, can be tuned by proper choice of the B concentration in these rapidly solidified alloys. It is worth to note that the increase in the Al content in the Fe–Al–B system can considerably improve the strength, while only indistinctively decreasing the plasticity. As typical examples, the compressive engineering stress–strain curves for $Fe_{85-x}Al_xB_{15}$ (x = 10, 20, 30) are shown in Fig. 2(a). It is well known that the improvement of strength can be explained by the mechanism of substitutional solid-solution strengthening [18]. When Al solute atoms are introduced in the Fe solid solution, local stress fields can

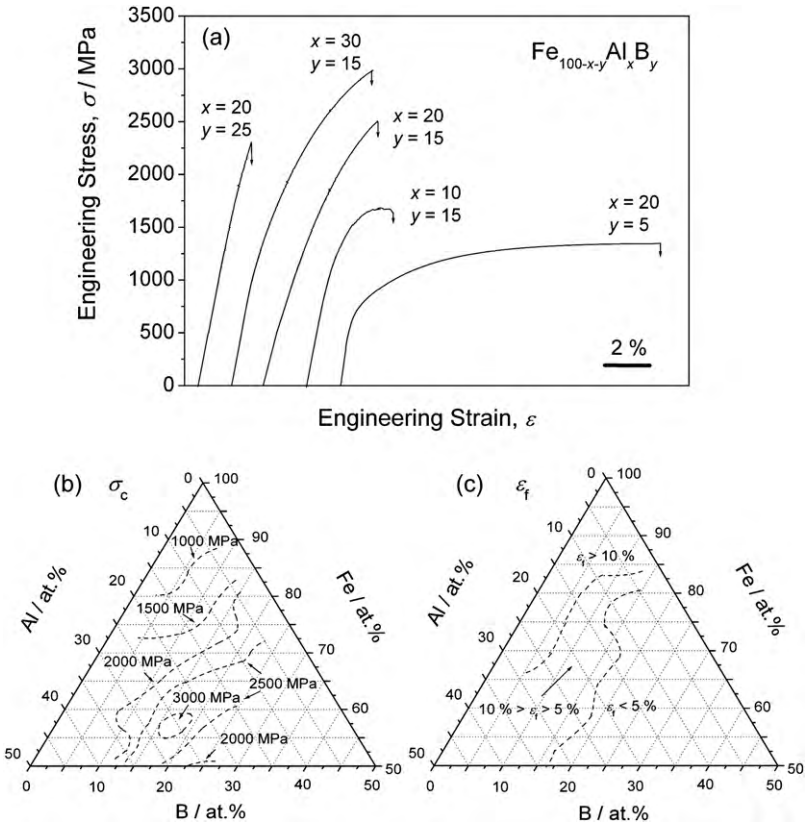

Fig. 2. (a) Typical compressive engineering strain–stress curves for Fe–Al–B alloys and contour maps of compressive strength (b) and fracture strain (c) in the Fe–Al–B ternary system showing the dependence of the mechanical properties on the B and Al content.

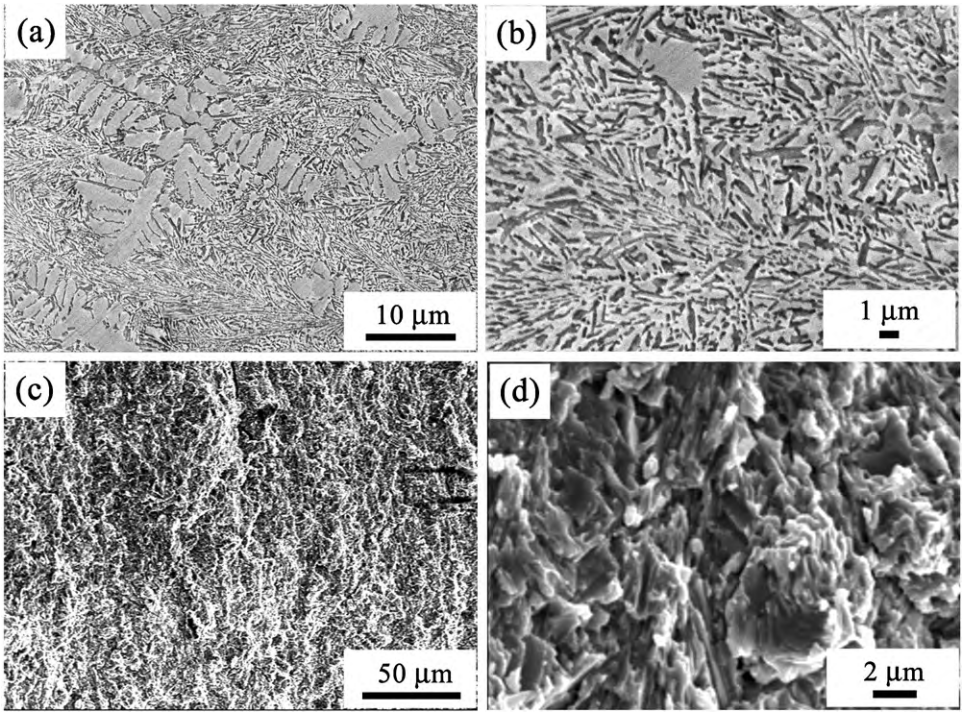

Fig. 3. Typical cross-sectional microstructural images for the $Fe_{55}Al_{30}B_{15}$ alloy at low (a) and high (b) magnification, and characteristics of the fracture surface low (c) and high (d) magnification.

be formed which can impede dislocation motion so as to increase the strength of the resulting alloys.

Contour maps of compressive strength (σ_c) and fracture strain (ε_f) in the Fe–Al–B system are shown in Fig. 2(b) and (c) according to the mechanical properties of all tested samples. Samples in the composition range of 10 at.% ≤ B ≤ 20 at.% and 55 at.% ≤ Fe ≤ 60 at.% display a high σ_c of ~3 GPa, which is comparable to the values found for Fe-based bulk metallic glasses [19,20], together with considerable plasticity (~5%). As a typical example, as-cast and fractured $Fe_{55}Al_{30}B_{15}$ samples were further studied by SEM. Fig. 3(a) and (b) shows the microstructure of the as-cast $Fe_{55}Al_{30}B_{15}$ alloy. An irregular ultrafine eutectic with a size below 1 μm can observed as matrix. Some undergrown ~10 μm-sized dendritic cores are embedded in this eutectic matrix. This kind of multiphase composite structure with excellent mechanical properties has been mentioned in many reports [1,2]. The fracture surface of this sample is shown in Fig. 3(c) and (d). Because the images show fracture characteristics similar to intergranular fracture on the 1 μm-scale, the cracks in this alloy should appear and propagate in the eutectic matrix. The similar deformation behavior of this type of material was also described in [2,8,9]. These contour maps can give a global view of the mechanical properties in the Fe–Al–B ternary system, which is useful for further research.

4. Conclusions

The constituent phases and mechanical properties of rapidly solidified $Fe_{100-x-y}Al_xB_y$ ($0 < x \leq 35$, $0 < y \leq 25$, and $x + y \leq 50$) ternary alloys were evaluated. Two crystalline phases of α-Fe(Al) solid solution and Fe_2B compound can be found in all samples. Contour maps of strength and deformability are plotted according to the compressive test results of the as-cast Fe–Al–B rods. The alloys can exhibit high compressive strength up to ~3 GPa together with considerable plasticity. The formation of ultrafine eutectics and solid-solution strengthening are responsible for the remarkable improvement of strength.

Acknowledgements

R. Li would like to acknowledge the fellowship support from the Alexander von Humboldt Foundation. Stimulating discussions with D.H. Kim, G. Liu, U. Siegel and G. Wang are also gratefully acknowledged.

References

[1] G. He, J. Eckert, W. Löser, L. Schultz, Nat. Mater. 2 (2003) 33–37.
[2] J. Eckert, G. He, J. Das, W. Löser, Mater. Trans. 44 (2003) 1999–2006.
[3] Y. Li, K. Georgarakis, S.J. Pang, F. Charlot, A. LeMoulec, S. Brice-Profeta, T. Zhang, A.R. Yavari, J. Mater. Res. 24 (2009) 1513–1521.
[4] J.M. Park, N. Mattern, U. Kühn, J. Eckert, K.B. Kim, W.T. Kim, K. Chattopadhyay, D.H. Kim, J. Mater. Res. 24 (2009) 2605–2609.
[5] U. Kühn, N. Mattern, T. Gemming, U. Siegel, K. Werniewicz, J. Eckert, Appl. Phys. Lett. 90 (2007) 261901.
[6] K. Werniewicz, U. Kühn, N. Mattern, B. Bartusch, J. Eckert, J. Das, L. Schultz, T. Kulik, Acta Mater. 55 (2007) 3513–3520.
[7] J.M. Park, S.W. Sohn, D.H. Kim, K.B. Kim, W.T. Kim, J. Eckert, Appl. Phys. Lett. 92 (2008) 091910.
[8] J.M. Park, K.B. Kim, W.T. Kim, M.H. Lee, J. Eckert, D.H. Kim, Intermetallics 16 (2008) 642–650.
[9] J.M. Park, K.B. Kim, W.T. Kim, D.H. Kim, Appl. Phys. Lett. 91 (2007) 131907.
[10] J.M. Park, S.W. Sohn, T.E. Kim, K.B. Kim, W.T. Kim, D.H. Kim, Scripta Mater. 57 (2007) 1153–1156.
[11] R. Li, G. Liu, M. Stoica, J. Eckert, Intermetallics 18 (2010) 134.
[12] M. Palm, Intermetallics 13 (2005) 1286–1295.
[13] R. Krein, A. Schneider, G. Sauthoff, G. Frommeyer, Intermetallics 15 (2007) 1172–1182.
[14] C.G. McKamey, J.H. Devan, P.F. Tortorelli, V.K. Sikka, J. Mater. Res. 6 (1991) 1779–1805.
[15] A. Taylor, R.M. Jones, J. Phys. Chem. Solids 6 (1958) 16–37.
[16] V. Raghavan, Phase Diagrams of Ternary Iron Alloys, Indian Institute of Metals, Calcutta, 1992.
[17] T.B. Massalski, H. Okamot, R.P. Subramanian, L. Kacprzak, Binary Alloy Phase Diagrams, 2nd ed., ASM International®, United States, 1991.
[18] F.R.N. Nabarro, Theory of Crystal Dislocation, Oxford University Press, Oxford, 1967.
[19] A. Inoue, Acta Mater. 48 (2000) 279–306.
[20] T. Zhang, F.J. Liu, S.J. Pang, R. Li, Mater. Trans. 48 (2007) 1157–1160.